Conf-950828--12

SAND95-1107C

Observations of the Boiling Process from a Downward-Facing Torispherical Surface: Confirmatory Testing of the Heavy Water New Production Reactor Flooded Cavity Design

T.Y. Chu, J.H. Bentz, and R.B.Simpson
Sandia National Laboratories
Albuquerque, New Mexico 87185

Accepted for Presentation
at
30th National Heat Transfer Conference
Portland, Oregon
August 5-9, 1995

Abstract

Reactor-scale ex-vessel boiling experiments were performed in the CYBL facility at Sandia National Laboratories. The boiling flow pattern outside the RPV bottom head shows a center pulsating region and an outer steady two-phase boundary layer region. The local heat transfer data can be correlated in terms of a modified Rohsenow correlation.

DISCLAIMER

DISCLAIMER

Portions of this document may be illegible in electronic image products. Images are produced from the best available original document.

The flooded cavity is an accident management feature in the design of the heavy water new production reactor (HWR-NPR) [1] as well as some advanced light water reactors (ALWRs) such as the AP-600. This accident management concept is also being considered for applications in existing light water reactors (LWRs) [2,3,4,5]. The success of the flooded cavity concept depends on the effectiveness of the ex-vessel boiling process in dissipating the decay heat imposed by the molten core on the reactor vessel bottom.

The ex-vessel boiling process is unique in that boiling takes place outside of a large downward-facing curved surface. Because of the upside-down geometry, the vapor generated in boiling cannot readily rise away from the heating surface; rather, it must flow along the surface to the edge of the surface before it is released into the bulk liquid. This gives rise to the possibility that the boiling process might be scale dependent [6,7].

The ex-vessel boiling process can be described as boiling from a large downward-facing curved surface. There is experimental evidence from laboratory-scale experiments that boiling in a downward-facing configuration depends on both surface inclination [8,9] and scale [10]. Nishikawa's classical experiment [8] on boiling from an inclined downward-facing flat plate shows that at low heat fluxes (<70 kW/m^2), the effectiveness of nucleate boiling heat transfer increases as the surface inclination increases (toward horizontal), but at high heat fluxes (>170 kW/m^2), heat transfer is essentially independent of surface inclination. Other flat plate experiments confirm the general trend of this observation [9,11]. Data from experiments ranging from cryogenic fluid [12,13] to water [14] show that the critical heat flux (CHF) decreases monotonically as the surface inclination varies from horizontally upward-facing through vertical to horizontally downward-facing. The deterioration of CHF accelerates as the surface inclination approaches horizontally downward-facing. Anderson and Bova [10] measured the CHF of downward-facing circular disks with diameters ranging from 0.05 m to 0.3 m, in Freon-11. Their data suggest that CHF is inversely proportional to disk diameter.

There have been a number of recent experiments specifically designed to investigate downward-facing boiling in connection with the flooded cavity design. The transient quenching integral experiments of Henry et al. [2] demonstrate that for highly subcooled water, nucleate boiling heat flux from a 0.3-m-diameter curved surface exceeds 1 MW/m^2. Theofanous et al. [15] investigated the variation of CHF in an AP-600-like configuration in the ULPU-2000 facility. ULPU-2000 is a steady-state boiling facility; the bottom head of the reactor vessel is represented by 30° segments of 0.15-m wide, two-dimensional slices of the bottom head geometry. The CHF at the bottom center region, under pool boiling conditions (without a large gravity head), is found to be approximately 300 kW/m^2. The quenching experiment by Chu et al. [16,17,18] using

* This work was performed at Sandia National Laboratories and supported by the U.S.Department of Energy under Contract No. DE-AC04-76-DP00789.
DE-AC04-94AL85000.

0.61-m-diameter cylindrical slugs, with flat and curved surfaces, shows critical heat flux from downward-facing surfaces to be in the range of 400-600 kW/m^2. Cheung and Haddad [19] and Cheung et al. [20] investigated boiling from hemispheres using test sections of up to 0.3 m in diameter under both transient quenching and steady-state conditions in saturated and subcooled water. The critical heat flux for saturated boiling obtained from transient quenching experiments is found to be 400 kW/m^2 in the bottom center region and increases substantially away from this region.

EXPERIMENTAL APPARATUS - THE CYBL FACILITY

CYBL, the Cylindrical Boiling Facility, was developed under the Department of Energy's (DOE) New Production Reactor Program to perform confirmatory experiments for the flooded cavity design for the heavy water new production reactor. The DOE's Office of Nuclear Energy continued to fund the CYBL facility to provide data for the assessment of the AP-600 flooded-cavity design.

CYBL has a tank within a tank design; the inner tank simulates the reactor pressure vessel; the outer tank simulates the reactor cavity (Figure 1). Both tanks are made of 316 L stainless steel, the proposed material for the HWR-NPR reactor vessel. The outer tank is 5.1 m in diameter and 8.4 m high. The test (inner) tank is 3.7 m in diameter and 6.8 m high. The diameter of a commercial power reactor is typically 4 m. Therefore, CYBL is essentially full scale. The inner and outer tanks are connected by a truncated cone section. The annular space between the two tanks measures 0.71 m and the distance between the bottom of the test tank and the bottom of the outer tank is 1.38 m. The bottom head of the test tank is formed from 14.3-mm (9/16 in) thick flat stock. There is a maximum thickness reduction of 12% at the knuckle region (to no less than 12.7 mm or 0.5 in) due to the forming process. The boiling surface is finished to a 125 finish and the entire exterior of the test tank is sandblasted with No. 180 aluminum oxide grit to "White Metal Finish" per SSPC-SP5 standard. Sessile drop observations made on a test coupon sandblasted together with the test vessel indicate that water wets the surface and that the contact angle is slightly less than 30°, at a surface temperature approximately 10 K within the saturation temperature.

Duplicating the design of the HWR-NPR reactor pressure vessel, the test tank has a torispherical head with a crown radius of 3.36 m and a knuckle radius of 0.66 m (Figure 2). The polar angle corresponding to the crown is 51.3° (25.65° on each side of the vertical central axis); therefore, the surface inclination at the junction between the crown and the knuckle is 25.65°. The arc distance (as measured from the bottom center) to the junction is 1.50 m and the surface inclination varies linearly from 0° to 25.65° from bottom center to the junction. The knuckle region corresponds to arc distances between 1.50 m and 2.25 m and the surface inclination varies linearly with arc distance between 25.65° and 90°. It is important to note that the facility is designed with enough flexibility to accommodate a test tank of any configuration with a cylindrical diameter less than 3.7 m.

The heat flux from the core debris on the bottom head is simulated with an array of radiant lamp panels. For the present experiments, twenty 0.3-m by 1.2-m panels are used. Each panel consists of a flat aluminum reflector and two bus bars for installing up to 63, 480-V, 6-kW linear quartz lamps. The reflector and bus bars are water cooled. The panels are organized into twelve individually controlled heating zones. By adjusting the power input to each zone, the density of lamps in each panel, and the three-dimensional configuration of the panel array, the heat flux distribution on the bottom head can be tailored. For the present series of experiments, the panels were assembled as a horizontal planar array located approximately 1 m above the bottom (center) of the test vessel. Currently, the maximum total test power available is 4.3 MW; however, the test power can be increased to 6 MW by upgrading the cables between the substation and the power supply. The maximum achievable heat flux determined from system design experiments is 400 kW/m^2.

The CYBL test apparatus is installed over an observation pit. There are 51 viewing windows, ranging in size from 0.3 m to 0.6 m in diameter, on the side and bottom of the outer vessel for observing the boiling process. Arrays of thermocouples are used to measure the surface and in-depth temperatures of the test vessel. Heat fluxes are calculated from temperatures measured at the surface and 9.5 mm into the surface. Five thermocouples located 0.15 m away from the crown portion of the bottom head are used to measure the bulk temperature of the water. A thermocouple tree, up the annulus between the tanks, monitors the temperature of the water and steam at 15 vertical locations. All except the surface thermocouples are 1.6-mm (1/16 in), sheathed, type K thermocouples with grounded junctions. The in-depth thermocouples are installed in holes drilled into the test surface from the water side. The thermocouples are dipped in an indium/gallium/tin liquid (at room temperature) metal alloy before installation. The wetting characteristics of the indium/gallium/tin alloy

allow the gap between the thermocouple and the hole to be totally filled with the alloy, providing excellent thermal contact. Heat conduction calculations show that the error in the temperature gradient that is due to the along-the-gradient installation of the thermocouples is no more than 4%. The surface thermocouples are intrinsic thermocouples made from the same 1.6-mm sheathed thermocouples, with the last 25 mm stripped to bare wires. The two bare wires are welded individually onto the test surface typically 2-3 mm apart. This installation lessens the bulk (0.3-mm-wire vs. 1.6-mm-sheath) of the sensor on the surface and provides a locally (3 mm) averaged surface temperature.

A deionization system with ultraviolet sterilization lamps and deaerator provides the water for the experiment. The water has a typical resistance of 200-400 MΩ/m. Two 72-kW electrical immersion heaters are used to heat the water to the desired temperature for an experiment. The heaters are also used to boil and to de-aerate the water before an experiment. Steam generated during the experiment is piped to a water-cooled condenser by two 0.2-m steam pipes attached to the truncated cone transition section between the two tanks. The condensate is collected and reheated in an intermediate tank equipped with a 72-kW electrical immersion heater before being returned to the test apparatus. A "U" tube filled with water is used as pressure/vacuum protection blowout for the apparatus.

Because of safety considerations, the experiment is conducted remotely. A ten-camera video system is used to observe and record the boiling process. Video cameras are also used to monitor the operation of key systems in the facility. In addition to temperature and power, water flow rates and system pressure are measured. The data acquisition and control system can generate plots of temperature and heat flux at selected locations and provide operational information on key systems in real time. The control system can "scram" the test power within 2 seconds should thermocouples indicate a departure from nucleate boiling. It is also possible to scram the test power manually from the control console based on visual (via TV cameras) or other indications.

OBSERVATIONS OF THE EX-VESSEL BOILING PROCESS

A total of ten experiments were performed [17,18] in the CYBL facility. Uniform as well as edge-peaked heat flux distributions were tested. The edge-peaked distribution arises from molten core convection in the bottom head [21,22,23]. The nominal heat flux for the experiments varied from 60 kW/m^2 to 200 kW/m^2.

For all the experiments, the water level was 5 m above the bottom center of the test vessel. Because of the 5 m of gravity head, the bulk condition in the vicinity of the bottom head is subcooled. In all the experiments, the entire bottom head is in subcooled nucleate boiling. The subcooling corresponding to a 5 m static head is 12 K, but the actual observed subcooling of the bulk water (as measured 0.15 m under the bottom center region) varies from approximately 9 K to 10 K. The lower subcooling corresponds to higher heat flux experiments. The reduction in subcooling can be attributed to convective mixing due to the flow induced by the boiling process.

Shown in Figures 3 and 4 are typical heat flux and surface superheat (based on local saturation temperature) distributions for uniform heat flux and edge-peaked heat flux experiments. The temperature distributions plotted are from two radial ("meridian") thermocouple arrays 7.5° apart. The general trend in the effectiveness of boiling heat transfer as a function of surface location can be obtained by examining the variation of surface superheat as a function of surface location for a uniform heat flux experiment, as shown in Figure 3 for Run NE1-A. In the region where the heat flux is essentially constant (0-1.8 m), the surface superheat decreases with arc distance (surface inclination); however, beyond 1.8 m, despite the decrease in heat flux, the surface superheat increases with arc distance up to the vicinity of the rim of the bottom head. More detailed discussions of surface superheat and heat transfer coefficient will be given in the next section. We now turn our attention to the phenomenology of ex-vessel boiling.

The boiling process in the bottom center region is cyclic in nature with four distinct phases: direct liquid/solid contact, bubble nucleation and growth, formation of vapor masses by lateral coalescence of bubbles and vapor masses, and vapor mass dispersion. The flow pattern is axisymmetric with the flow generally in the radial direction. Selected video frames of the boiling flow pattern for a test at approximately 140 kW/m^2 are shown in Figure 5; the field of view is slightly more than 2 m and the white bar on the lower right of Plate 1 is 0.3 m (12 in). Each plate in Figure 5 is 1/15 second apart. Plate 2 corresponds to the end of the coalescence phase, and the vapor mass at the bottom center area reaches its maximum size (approximately 1 m). Plate 3 is the start of the dispersion phase where the center vapor mass moves out, radially opening up a circular bare center region with direct liquid/solid contact. New bubbles appear within one frame (1/30 second) of the video record. With time, the dispersing vapor mass continues to expand in the form of a ring, exposing more areas to direct liquid/solid

contact. The expansion gives rise to an orderly progression of the four phases in the radial direction. In time, the center vapor mass grows to maturity and disperses, repeating the cycle. In Figure 6 the pulsation frequency for all the experiments performed to date is plotted against the averaged heat flux over a 2-m radius around the bottom center of the test vessel. At low heat fluxes, the pulsation frequency increases with heat flux. However, beyond a certain heat flux, the frequency stays essentially constant. While the data are too sparse in the low heat flux region to exactly define the low and high heat flux region, it appears that the demarcation is around 100 kW/m^2. It is interesting to note that this heat flux range corresponds to a change in the slope of the boiling curve from the quenching experiments by Chu et al. [16,18]. Similar to the trend in frequency, the size of the vapor mass also increases with heat flux (see Figure 7). The data in Figure 7 must be considered to be preliminary because each point represents only a single measurement of the diameter of a vapor mass. We are in the process of acquiring image processing capability by which large numbers of frames can be examined in greater detail.

An examination of the texture of the center vapor mass in Figure 5 shows that it is not a monolithic single vapor mass; rather, the vapor mass consists of a collection of coalescing vapor masses with a typical size of tens of centimeters. The details of the formation of the vapor mass are obtained from 16-mm movies of the central region of the bottom head. The initial growth of the center vapor mass for a heat flux of approximately 180 kW/m^2 is shown in Figure 8. The frames are 0.05 second apart. An expanding circular region of direct liquid/solid contact is clearly shown. Of particular interest is the much finer texture of the photograph compared with video records of similar magnification, although video records are capable of reproducing similar textures. The difference is due to the different lighting conditions for the video and the movie. The movie was taken with extra lighting and we believe that the images correspond to near surface conditions rather than the surface (envelope) of the vapor mass. What the movie shows are individual nucleating sites (white dots against the gray background in Figure 8) that feed the envelope of the vapor mass. These preliminary observations suggest a picture of downward-facing nucleate boiling similar to that observed by Gaertner [25] for nucleate boiling on an upward-facing surface and adapted by Haramura and Katto [26] to model critical heat flux. Gaertner pictured vapor masses (mushrooms) "hovering over" the heated surface (Figure 9a). In the downward-facing case, relatively flat vapor masses are "hovering against" the heated surface (Figure 9b). For the one case of a heat flux of 180 kW/m^2, by counting an area of 0.1 m by 0.1 m, the nucleating site density, n, was estimated to be in the range of 6-8$\times 10^3$/m^2. This active site density is a factor of 2 to 3 less than that obtained by Gaertner and Westwater [27] for the same heat flux, on an upward-facing copper surface. The site density is one order of magnitude less than that observed by Wang and Dhir [28] from a vertical copper surface. Taking $(n)^{0.5}$ as the measure of distance between sites, the site-to-site distance is then estimated to be 11-13 mm.

Shown in Figure 10 is an example (run NE2-E, average heat flux 187 kW/m^2) of the dynamics of the growth of the center vapor mass as well as the dispersing ring. The diameters of the center vapor mass (Dp) and the ring (Dri and Dro) are plotted against frame number and each frame is 1/30 second apart. At time zero, the center patch (vapor mass) is just beginning to nucleate and the diameter of the newly formed bare spot of direct liquid/solid contact (Dri - the inner diameter of the dispersing ring) is approximately 0.3 m; the outer diameter of the dispersing ring (Dro) is approximately 1.15 m. The center patch becomes fully grown in 15 frames or 0.5 second, which is the period of the pulsation. The full-grown center patch has a diameter of approximately 1.12 m. By the 16th frame, the cycle repeats itself with the opening up of the center patch into a ring, with a diameter slightly larger than the full-grown center patch. The average expansion speed of the radius of the patch and the ring's inner and outer perimeters are calculated to be 1.2 m/sec, 1.5 m/sec, and 1.0 m/sec, respectively. These expansion speeds increase with heat flux; between the lowest (NE2-A, 57.4 kW/m^2) and the highest heat flux runs (NE1-C, 188 kW/m^2) the speeds vary less than 35%. It is useful to note that these speeds are small compared with the critical speed ($\approx$ 8 m/sec) for stratified horizontal flow instability. It is also important to realize that the expansion of the center vapor mass (patch) is not that of a contact line associated with the expansion of a monolithic vapor envelope. The growth is related to the sequential nucleation and lateral coalescence of bubbles and vapor masses, i.e., the center patch grows mostly because of the addition of newly formed bubbles and vapor masses around the perimeter.

As the dispersing ring travels outward and upward along the bottom head contour, it also sweeps away individual bubbles along its path. Eventually, the ring breaks into segments. The broken flat ring segments have a tendency to retract in length and thicken. The thickened segments maintain the original direction of travel for up to about 0.3 m, then condense rather suddenly in the surrounding subcooled water. It is possible that when a

vapor segment contracts and thickens it protrudes away from the boundary layer of supersaturated water next to the heated surface. Figure 11 is a side view of the lower portion of the test vessel; a thickened ring segment is clearly visible near the left edge of the profile of the bottom head. The condensation zone is approximately 0.3 m beyond that location. The radial location of the condensation zone is quite well defined; the corresponding radius increases with heat flux. As a result of the vapor mass condensation process, visually the boiling process beyond the condensation zone appears to a large degree to be decoupled from the cyclic pulsation of the bottom center region and is observed to be essentially a steady two-phase boundary layer flow (Figure 12). The vapor generated in the outer region also condenses in the bulk subcooled water a very short distance beyond/above the rim of the bottom head. The 4-m high annular region around the side of the test vessel is essentially occupied by single-phase subcooled liquid to within about 0.6 m of the water-steam interface. Intense bulk vaporization takes place in the top 0.3 m of the water. Figure 13 is a schematic representation of the key observations of the ex-vessel boiling process.

INITIAL ASSESSMENT OF CYBL EXPERIMENTS - A CORRELATIONAL APPROACH

Observations of the phenomenology of ex-vessel boiling suggest that perhaps the bottom center region can be modeled as a surface renewal phenomenon and the outer region can be modeled as a steady two-phase boundary layer. We leave these efforts for the future. In this section, we simply attempt to correlate the CYBL heat flux and temperature data. We investigate the possibility of using a Rohsenow-like correlation because of its relative simplicity and general utility.

As pointed out by Liaw and Dhir [29], the Rohsenow [30] boiling correlation "though not based on sound reasoning of physical mechanisms, has been very successful in predicting the observed nucleate boiling data.... One reason for the success of this [Rohsenow] correlation is that it combines a correct length scale with the appropriate thermophysical properties." The general form of the Rohsenow correlation can be written as:

$$\frac{\Delta T\, Cp_l}{h_{fg}} = Csf\left\{\left(\frac{q}{\mu_l\, h_{fg}}\right)\left[\frac{\sigma}{g\,(\rho_l-\rho_v)}\right]^{1/2}\right\}^{r} \mathrm{Pr}^{n} \qquad (1)$$

where ΔT is the surface superheat, Cp_l is the liquid specific heat, h_{fg} is the latent heat, q is the surface heat flux, μ_l is the liquid density, ρ_l and ρ_v are the liquid and vapor density respectively, Pr is the Prandlt number, and σ is the surface tension.

The term

$$\left[\frac{\sigma}{g(\rho_l-\rho_v)}\right]^{1/2} \qquad (2)$$

is the standard surface tension length scale for boiling. Using typical water property values, the term takes a value of 2.5 mm. However, as observed in the video film of the boiling process in the CYBL experiments, the vapor masses on the underside of the vessel head are much larger than this scale. Furthermore, the scale of the vapor masses typically increases as the surface inclination approaches horizontal, i.e., the vapor masses increase in size from the rim of the bottom head toward the bottom-center of the head. It is, therefore, reasonable to use a trial function for the scale of the form

$$\left[\frac{\sigma}{g\sin\theta_i(\rho_l-\rho_v)}\right]^{1/2} \qquad (3)$$

where θ_i is the surface inclination above horizontal. The expression is singular for the bottom center location. This difficulty will be treated later in the development of the correlation.

Observations made in the present experiment and quenching experiments of Chu et al. [16,18] suggest that there are two regimes of nucleate boiling. In the low heat flux regime, coalescence of vapor masses is less complete and the pulsation rate increases with heat flux. In the high heat flux regime, coalescence produces large vapor masses and the pulsation rate is essentially constant. It is reasonable to assume that the low heat flux regime is analogous to the isolated bubble regime in upward-facing boiling and the high heat flux regime is analogous to the fully developed nucleate boiling regime. We will try to correlate the data from the high heat flux regime using a modified Rohsenow-like correlation with the variable local scale:

$$\frac{\Delta T\, Cp_l}{h_{fg}} = Csf\left\{\left(\frac{q}{\mu_l\, h_{fg}}\right)\left[\frac{\sigma}{g\sin\theta_i(\rho_l-\rho_v)}\right]^{1/2}\right\}^{r} \mathrm{Pr}^{n} \qquad (4)$$

The equation is singular at bottom center, where θ_i is zero. To avoid this problem, we make the assumption that the boiling curves are substantially the same for a horizontal

surface and for a surface of small inclination ($\theta < \theta m$). This assumption is consistent with the results of the quenching experiments of Chu et al. [16,18].

To complete the correlation, it will be necessary to fix the exponent r, the constant Csf, and the value of θm. Since the Prandlt number is not varied in the present experiment, we elect to take the standard value of 1 for the exponent n. In choosing the exponent r, we restrict the value to be the reciprocal of an integer. The following correlation, with $\theta m = 3°$, has been found to best represent the experimental data for surface heat flux greater than 100 kW/m^2:

$$\frac{\Delta T\, Cp_l}{h_{fg}} = 0.0116 \left\{ \left(\frac{q}{\mu_l\, h_{fg}} \right) \left[\frac{\sigma}{g \sin\theta_i (\rho_l - \rho_v)} \right]^{1/2} \right\}^{1/3} \mathrm{Pr} \qquad (5)$$

The exponent $r = 1/3$ is the same as the standard Rohsenow correlation [31] for the water/stainless steel pair. The coefficient $Csf = 0.0116$ is not too different from the 0.013 value in the standard Rohsenow correlation. Part of the difference can be attributed to the fact that the present experiment was somewhat subcooled. Because it was essentially constant, no attempt is made to include subcooling in the data correlation. The above equation is found to fit the surface superheat data for surface inclinations between 0 and 54°, with a standard deviation of ±7.4%. The value of 54° is not the result of a precise evaluation; it simply corresponds to the last thermocouple location where the correlation is found to apply. Beyond 54° (arc distance of 1.8 m), surface superheat variations with inclination change from decreasing with inclination to increasing with inclination (Figure 3); the correlation no longer applies. There are two possible contributions to this change of behavior. Measurements indicate that there is an increase in bulk temperature near these locations owing to vapor condensation beyond the rim of the bottom head. The accumulation of upstream vapor may also contribute to the decrease in the effectiveness of heat transfer in the near rim location. Figure 14 is a plot of the ratio of the experimental values of the surface's superheat and the values given by the correlation as a function of surface inclination. Most of the data are within ±12% of the correlation.

An expression for the heat transfer coefficient can be derived from Equation (5):

$$h = \frac{q}{\Delta T}$$

$$h = \frac{Cp_l\, q}{0.0116\, h_{fg}} \left\{ \left(\frac{q}{\mu_l\, h_{fg}} \right) \left[\frac{\sigma}{g \sin\theta (\rho_l - \rho_v)} \right]^{1/2} \right\}^{-1/3} \mathrm{Pr}^{-1} \qquad (6)$$

A comparison of the experimental data presented in Figures 3 and 4 and the correlations for surface superheat and heat transfer coefficients is shown in Figures 15 and 16. The data for run NE2-A are not used in the comparison because the heat flux level is below 100 kW/m^2. The agreement is good for both uniform heat flux and edge-peaked heat flux cases. Before leaving this section, it is useful to note that for the correlation to be of more general utility, it needs to be tested against a wider range of data.

CONCLUDING REMARKS

The heat dissipation requirements for the heavy water new production reactor are estimated to be 160 kW/m^2 [1]. Therefore, from the result of the present experiment, one can conclude that the flooded cavity design for the new production reactor will be able to dissipate the expected heat load in the event of a core meltdown accident.

The ex-vessel boiling process is subcooled nucleate boiling. The subcooling is mainly due to the gravity head of the water flooding the annular region between the reactor vessel and the cavity. The boiling flow consists of two regions: an inner cyclic/pulsating region and an outer, steady, two-phase boundary layer flow region. Condensation is observed at the edge of each region. Visually, the two regions are to a large degree decoupled. Because of condensation, there is not a continuous accumulation of upstream vapor toward downstream locations.

The center cyclic/pulsation pattern has four distinct phases: direct liquid/solid contact; bubble nucleation and growth; formation of vapor mass by lateral coalescence of bubbles and vapor masses; and vapor mass dispersion. The nucleate boiling process can be divided into two regimes: a low heat flux regime in which the pulsation rate increases with heat flux, and a high heat flux regime in which the pulsation rate is essentially constant. Preliminary observations of the boiling process suggest that similar to upward-facing boiling, the downward-facing boiling process consists of a large number of nucleation sites feeding large vapor envelopes (vapor masses) "hovering against" the heating surface. Although the frequency of vapor mass dispersion is essentially constant at high heat fluxes, the diameter of the center vapor patch (mass) tends to increase with heat flux. Therefore, it appears that the dispersion mechanism is not driven by the maturing of a vapor mass -

i.e., vapor mass dispersion is not the direct result of the center vapor mass reaching a certain critical size.

At this point, it is useful to compare some of the current experiments in ex-vessel boiling. Cheung and Haddad [19] and Cheung et al. [20] investigated the ex-vessel boiling process using hemispheres up to 0.3 m in diameter. Both transient and steady experiments have been performed; however, thus far, all the quantitative data come from quenching experiments. In the quenching process, film boiling, transition boiling, critical heat flux, and nucleate boiling coexist on the hemisphere and "there is significant local variation of the two-phase boundary layer configuration along the hemisphere" [20]. Therefore, the CHF values obtained in the quenching experiment must be viewed with some caution as they do not include the influence of prototypic vapor production over the hemisphere. In the ULPU experiments [15], attempts were made to simulate an axisymmetric geometry with a two-dimensional channel by matching upstream vapor production and superficial vapor velocity at the test location to what might be expected in an axisymmetric geometry. However, the flow-divergent effect outside of an axisymmetric body and the interaction between the "pool" convective flow and the boiling flow could not be duplicated in the two-dimensional channel geometry.

The CHF values obtained by the two sets of experiments are compared below:

	0°	30°	Exper. Method
Theofanous et al. [15]	280 kW/m^2	650 kW/m^2	2-D steady state
Cheung and Haddad [19]	400 kW/m^2	600 kW/m^{2*}	Quenching hemisphere

* Value obtained from interpretation of published data between 18° and 31.5°.

The CHF values obtained for the horizontal downward-facing inclination (0°) are substantially different. Perhaps the aforementioned nonprototypical experimental designs (with respect to the real reactor pressure vessel/cavity configuration) contributed to the difference in the CHF results between the experiment by Cheung et al. [20] and that by Theofanous et al. [15]. The values for the 30° inclination show much better agreement. This is not too surprising since scale and geometry effects are expected to be most important in near-horizontal, downward-facing configurations. In this connection, it is interesting to note that neither the Theofanous et al. [15] experiment nor that by Cheung and Haddad [19] and Cheung et al. [20] reports the regular cyclic/pulsation flow pattern that occurs at the bottom center area in the present experiment. It is also important to note that although the current CYBL test vessel bottom is torispherical, its crown region represents the hemispherical bottom center region of a typical pressurized water reactor with prototypical scale and geometry, and the bottom center region is where boiling is most sensitive to scale and geometry. The radius of curvature of the crown region is approximately 50% oversized (2.2 m versus 3.3 m); therefore, it may accentuate lower angle phenomena. However, it is difficult to imagine that being 50% oversized would drastically change the ex-vessel boiling phenomena.

The experiments described here show that the gravity head has an important influence on the ex-vessel boiling process. For the AP-600 bottom head, the bubbles experience a 5 K decrease in saturation temperature with a 2-m change in elevation, as they flow from the bottom center region to the rim of the bottom head. While the gravity head of the water in the annular region around the reactor vessel can be simulated in a laboratory-scale experiment by pressurization, the along-the-flow-path variation of the saturation temperature cannot be duplicated in such experiments. Therefore "local" observations from a laboratory-scale experiment are not likely to simulate prototypical "local" effects on a reactor scale because of a lack of correspondence in the variation of the "local" conditions. Of course, the importance of the lack of correspondence can only be ascertained by direct comparison of reactor-scale and subscale experiments. Another effect that is difficult to scale is the lateral coalescence of bubbles and vapor masses. As shown earlier, the typical site-to-site distance is on the order of 10 mm; thus it is doubtful that much lateral coalescence can take place at the bottom center region of a laboratory-scale experiment.

We have been reasonably successful in correlating the CYBL experiments using a Rohsenow-like formulation with a variable-length scale. The success of the correlation probably comes from the fact that condensation decreases the effects of the vapor accumulated upstream and the variable-length scale captures the trend of the vapor mass scale. Because of the limited range of data, the present correlation is best viewed as a correlation rather than a model.

The current set of experiments provides confirmatory data for the design of the flooded cavity for the new production reactor [1]. It also covers the baseline requirement for the AP-600 [2]. There are further experiments that are useful to pursue both in terms of the

basic phenomenology of ex-vessel boiling and plant design-specific issues.

Some of the phenomenology-related experiments are:

1. Wider heat flux range

   These experiments would establish the margin of safety of flooded cavity designs and provide a wider range of data for modeling the ex-vessel boiling process. The effect of flux distribution (as a result of melt convection) is also of interest in application and in modeling.

2. Effect of water level

   Water level is an important variable because it determines the degree of gravity subcooling and therefore the vapor mass condensation process. The effect of water level is also important for potential applications in existing light water reactors, where the amount of water for flooding can be limited [4].

As pointed by Okkonen [4] and Rouge and Seiler [5], in-vessel core retention by external flooding has many plant-specific issues. Some of the experiments that are of importance in applications are:

1. The effect of vessel penetrations

   Penetrations will affect the growth as well as the dispersion of vapor masses, especially in the bottom center region.

2. The effect of reactor insulation

   Reactor vessel insulation and, in the case of a boiling water reactor the vessel skirt, may present problems of steam relief as well as water ingression. Furthermore, observations made in the CYBL experiments indicate that the vigorous boiling/condensation process may result in substantial forces that may threaten the mechanical integrity of the reactor insulation.

3. Subcooling

   At the initial stage of flooding, the water flooding the cavity is greatly subcooled; therefore, the capacity for cooling is substantially higher. Aside from its phenomenological interest, the information on subcooling is important in accident management because it provides the data necessary to determine at what stage of the accident (how far down the decay curve) it becomes possible to take credit for ex-vessel boiling.

LITERATURE CITED

1. Jedruch, J., *Post-Melt Heat Flux Estimates in 670mwt NPR Lower RV Head*, NWRF-DOE-92-1483, EBASCO, Services Inc., New York, 1992.

2. Henry, R. E., and H. K. Fauske, *Nuclear Engineering and Design*, Vol. 139, pp. 31-43, 1993.

3. Henry, R. E., J. P. Burelbach, R. J. Hammersley, and C. E. Henry, *Nuclear Technology*, Vol. 101, pp. 385-399, 1993.

4. Okkonen, T., "In-vessel Core Debris Cooling through External Flooding of the Reactor Pressure Vessel," *Proceedings, OECD/CSNI/NEA Workshop on Large Molten Pool Heat Transfer*, Nuclear Research Center, Grenoble, France, 1994.

5. Rouge S., and J.M. Seiler, "Core Debris Cooling with Flooded Vessel or Core Catcher Heat Exchange Coefficients under Natural Convection," *OECD/CSNI/NEA Workshop on Large Molten Pool Heat Transfer*, Nuclear Research Center, Grenoble, France, 1994.

6. Chu, T. Y., R. C. Dykhuizen, C. E. Hickox, and B.L. Bainbridge, "Boiling from Downward Facing Surfaces with Application to the Flooded Cavity Concept," ANS Proceedings, HTC-Vol. 6, pp. 367-375, *1992 National Heat Transfer Conference*, San Diego, CA, 1992.

7. Chu, T. Y., R. C. Dykhuizen, and C. E. Hickox, *Scoping Studies of Boiling Phenomena Associated with the Flooded Cavity Design of the Heavy Water New Production Reactor*, SAND91-2383, NPRW-SA91-7, Sandia National Laboratories, Albuquerque, NM, 1993.

8. Nishikawa, K., Y. Fujita, S. Uchida, and H. Ohta, *International Journal of Heat Mass Transfer*, Vol. 27, pp. 1559-1571, 1984.

9. Guo, Z., and M. S. El-Genk, "An Experimental Study of the Effect of Surface Orientation on Boiling Heat Transfer During Quenching," *ASME Winter Annual Meeting*, Atlanta, GA, 1991.

10. Anderson, R.P., and L. Bova, *Transactions AmericanNuclear Society*, Vol. 14, pp. 294-295, 1971.

11. Chen, L.T., *Letters Heat Mass Transfer*, Vol. 5, pp. 111-120, 1978.

12. Vishnev, I.P., I.A. Filatov, Y.A. Vinokur, V.V. Gorokhov, and V.V. Svalov, "Study of Heat Transfer in Boiling of Helium in Surfaces with Various Orientations," *Heat Transfer - Soviet Research*, Vol. 8, No. 4, pp. 194-108, 1976.

13. Beduz, C., R. G. Scurlock, and A. J. Sousa, *Advances in Cryogenic Engineering*, Vol. 33, pp. 363-370, 1988.

14. El-Genk, M.S. and Z. Guo, "Saturated Pool Boiling from Downward-Facing and Inclined Surfaces," *Proceedings of The Engineering Foundation Conference on Pool and External Flow Boiling*, V.K. Dhir and A.E. Bergles Eds., pp. 243-249, Santa Barbara, CA, 1992.

15. Theofanous, T.G., S. Syri, T. Salmassi, O. Kymalainen, and H. Tuomisto, "Critical Heat Flux Through Curved, Downward Facing, Thick Walls," *Proceedings, OECD/CSNI/NEA Workshop on Large Molten Pool Heat Transfer*, Nuclear Research Center, Grenoble, France, 1994.

16. Chu, T. Y., J. H. Bainbridge, J. H. Bentz, and R. B. Simpson, *Observations of Quenching of Downward-Facing Surfaces*, SAND93-0688, Sandia National Laboratories, Albuquerque, NM, 1994.

17. Chu, T.Y., S.E. Slezak, J.H. Bentz, and W.F. Pasedag, "Large-Scale Boiling Experiments of the Flooded Cavity Concept for In-Vessel Core Retention," *Proceedings, OECD/CSNI/NEA Workshop on Large Molten Pool Heat Transfer*, Nuclear Research Center, Grenoble, France, 1994.

18. Chu, T. Y., J. H. Bainbridge, J. H. Bentz, R. B. Simpson, and S.E. Slezak, "Ex-Vessel Boiling Experiments - Laboratory and Reactor Scale Testing of the Flooded Cavity Concept for In-Vessel Core Retention," Submitted for Publication in Nuclear Engineering and Design, 1994.

19. Cheung, F. B., and K. H. Haddad, "Observation of the Dynamic Behavior of the Two-Phase Boundary Layers in the SBLB Experiments, *Proceedings of the 22nd Water Reactor Safety Meeting*, Bethesda, MD, 1994.

20. Cheung, F. B., K. H. Haddad, L. M. Charma, F. Otero, and A. L. Brundage, *Transactions American Nuclear Society*, Vol. 71, pp. 582-583, ANS Winter Meeting, Washington, DC, 1994.

21. Asfia, F.J., and V.K. Dhir, , "Natural Convection Heat Transfer in Volumetrically Heated Spherical Pools," *Proceedings, OECD/CSNI/NEA Workshop on Large Molten Pool Heat Transfer*, Nuclear Research Center, Grenoble, France, 1994.

22. Kymalainen, O., H. Tuomisto, O. Hongisto, and T.G. Theofanous, "Heat Flux Distribution from a Volumetrically Heated Pool with High Rayleigh Number," *Proceedings, NURETH 6*, Grenoble, France, pp. 47-53, 1993.

23. O'Brien, J. E., and G. L. Hawkes, "Thermal Analysis of a Reactor Lower Head with Core Relocation and External Heat Transfer," AIChE symposium Series 283, Vol. 87, pp. 159-176, *National Heat Transfer Conference*, Minneapolis, MN, 1991.

24. Chu, T.Y., J.H. Bentz, K.D. Bergeron, S.E. Slezak, and R.B. Simpson, "Large-Scale Testing of In-Vessel Debris Cooling Through External Flooding of Reactor Pressure Vessel in the CYBL Facility, *Transactions of the 21st Water Reactor Safety Information Meeting*, Bethesda, MD, 1993.

25. Gaertner, R.F., *Journal of Heat Transfer*, Vol. 15, pp. 401-428, 1965.

26. Haramura, Y., and Y. Katto, *International Journal of Heat Mass Transfer*, Vol. 26, pp. 389-399, 1983.

27. Gaertner, R.F., and J.W. Westwater, *Chemical Engineering Progress Symposium Series*, Vol. 59, pp. 52-61, 1960.

28. Wang C.H., and V.K. Dhir, *Journal of Heat Transfer*, Vol. 115, No. 3, pp. 659-669, 1993.

29. Liaw, S.P., and V.K. Dhir, *Journal of Heat Transfer*, Vol. 111, pp. 731-738, 1989.

30. Rohsenow, W.M., *Transactions of ASME*, Vol. 74, pp. 969-976, 1952.

31. Carey, V.P., *Liquid-Vapor Phase Change Phenomena*, Hemisphere Publishing, Washington, DC, 1992.

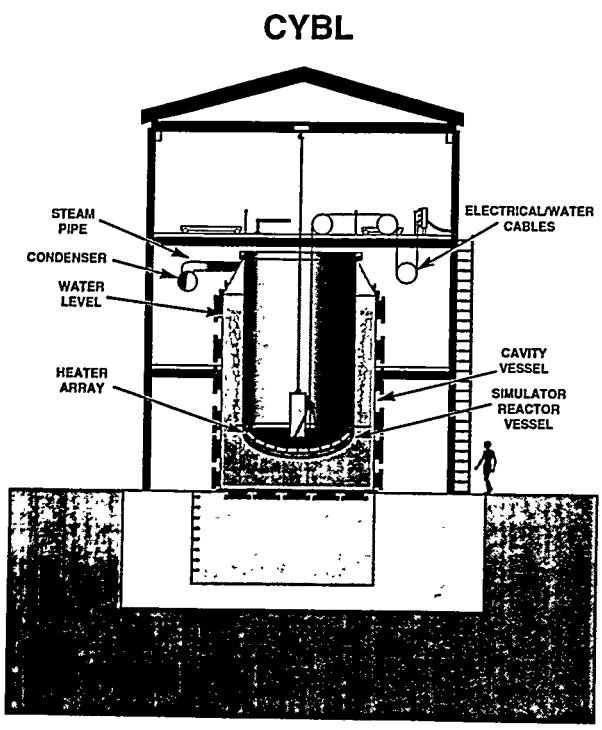

Figure 1. The CYBL facility.

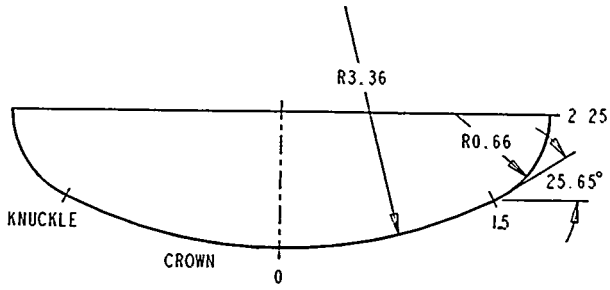

Figure 2. Shape of the test vessel bottom head.

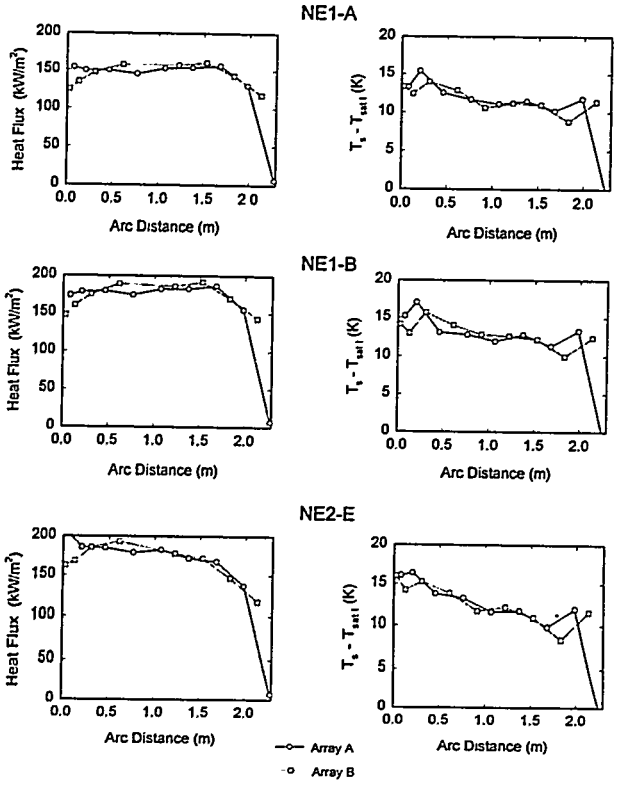

Figure 3. Heat flux and surface superheat for uniform heat flux cases.

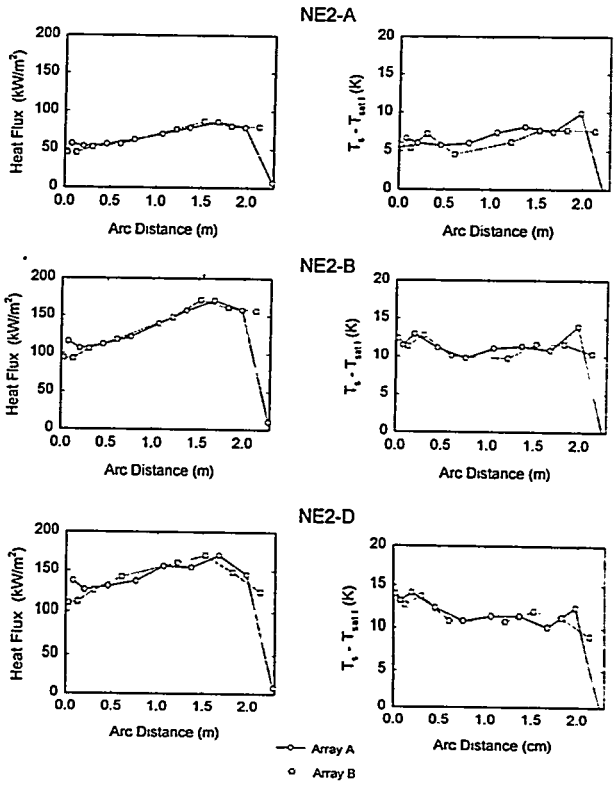

Figure 4. Heat flux and surface superheat for edge-peaked heat flux cases.

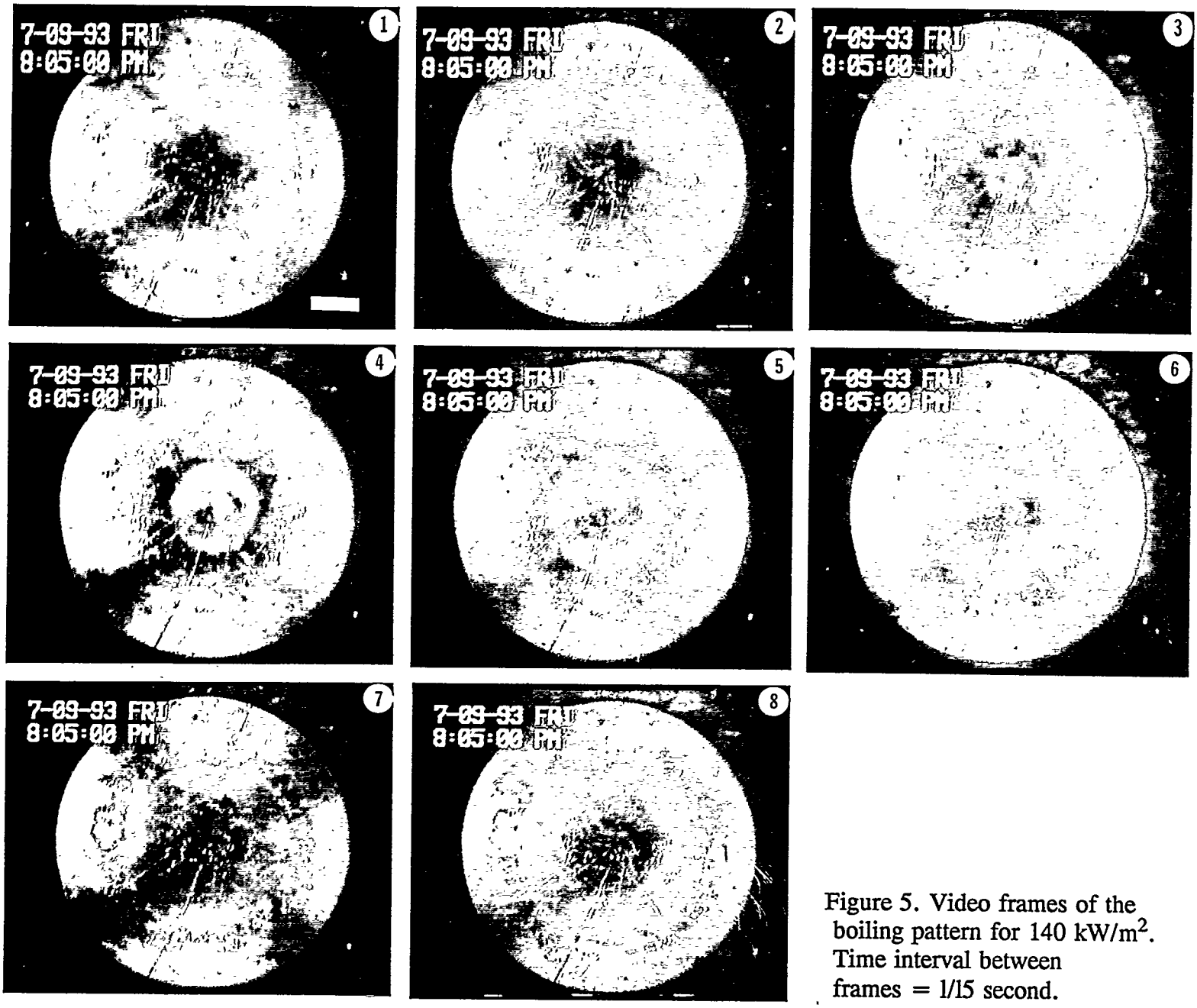

Figure 5. Video frames of the boiling pattern for 140 kW/m^2. Time interval between frames = 1/15 second.

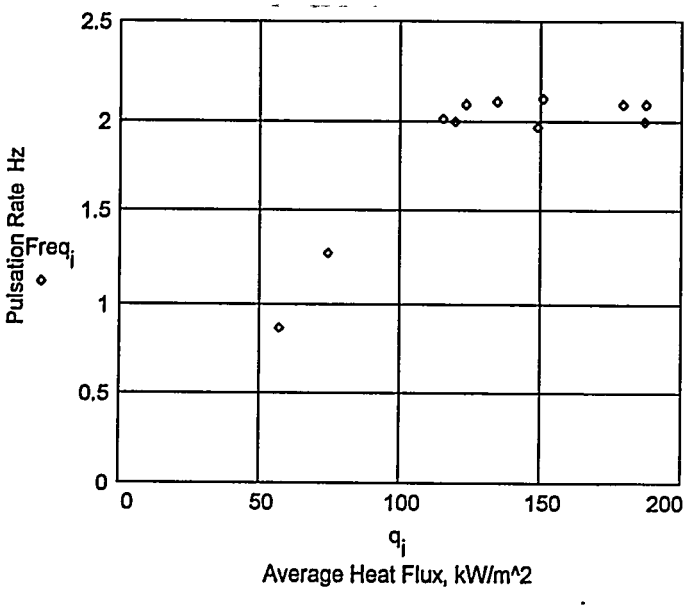

Figure 6. Pulsation frequency as a function of heat flux.

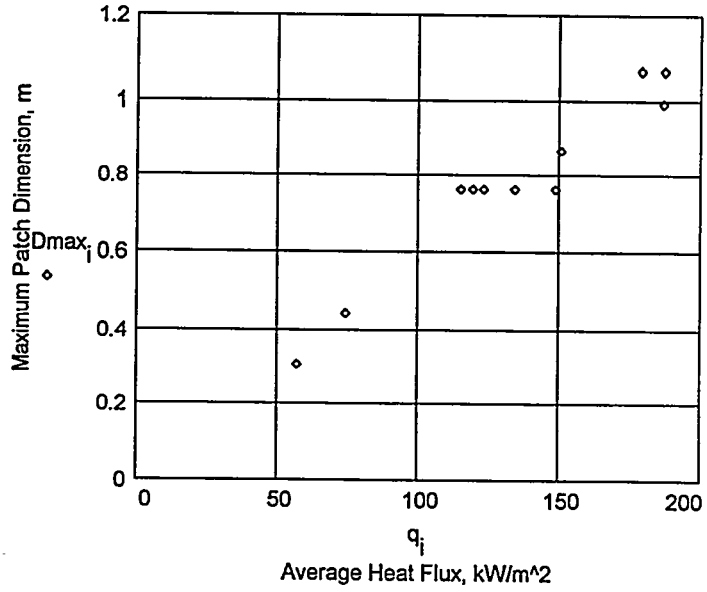

Figure 7. Size of the center vapor mass as a function of heat flux.

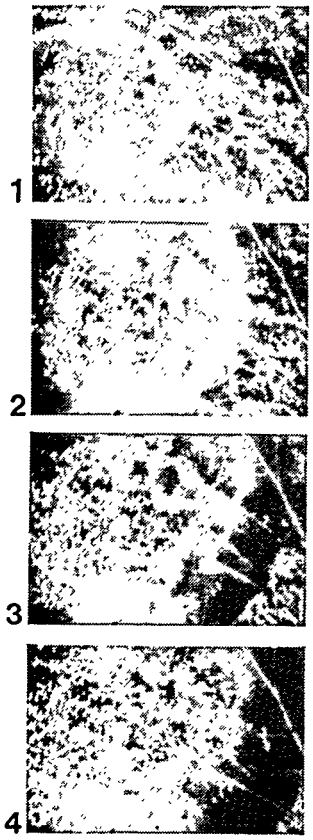

Figure 8. Boiling pattern from 16-mm film. Time interval between frames = 0.05 second.

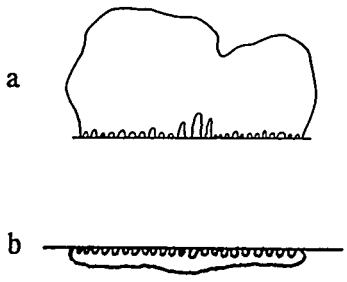

Figure 9. Comparison of upward-facing boiling (a) and downward-facing boiling (b).

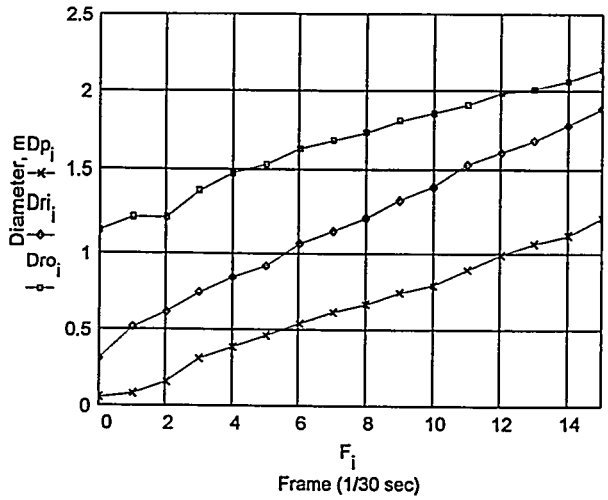

Figure 10. Growth of the center vapor mass and the dispersing ring.

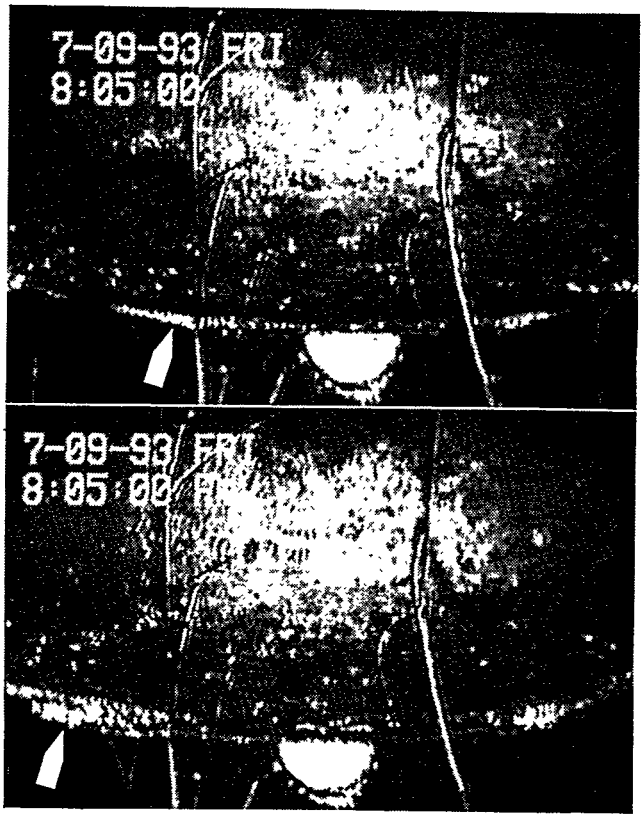

Figure 11. Boiling flow pattern around the bottom center region, side view.

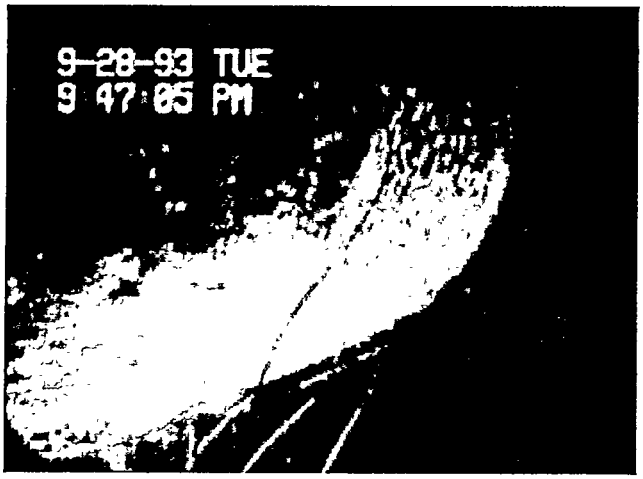

Figure 12. Boiling flow pattern around the knuckle region, side view.

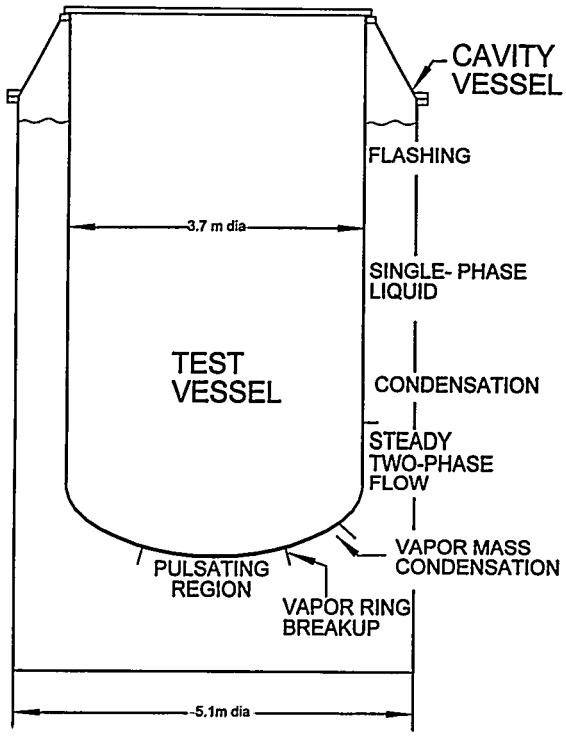

Figure 13. Schematic of key observations of the ex-vessel boiling process.

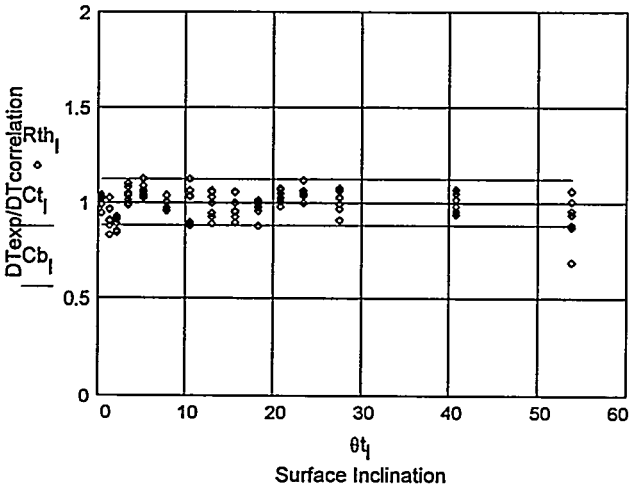

Figure 14. Overall comparison between the correlation and experimental data.

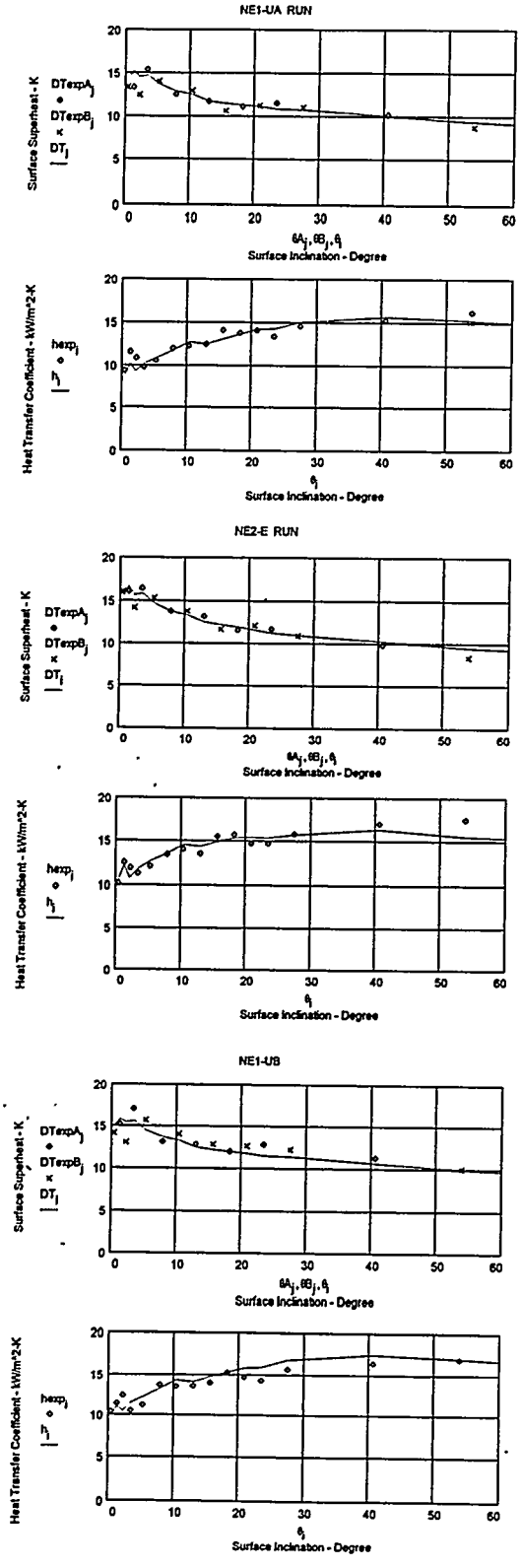

Figure 15. Comparison between the correlation and experimental data--surface superheat and heat transfer coefficient--uniform heat flux cases.

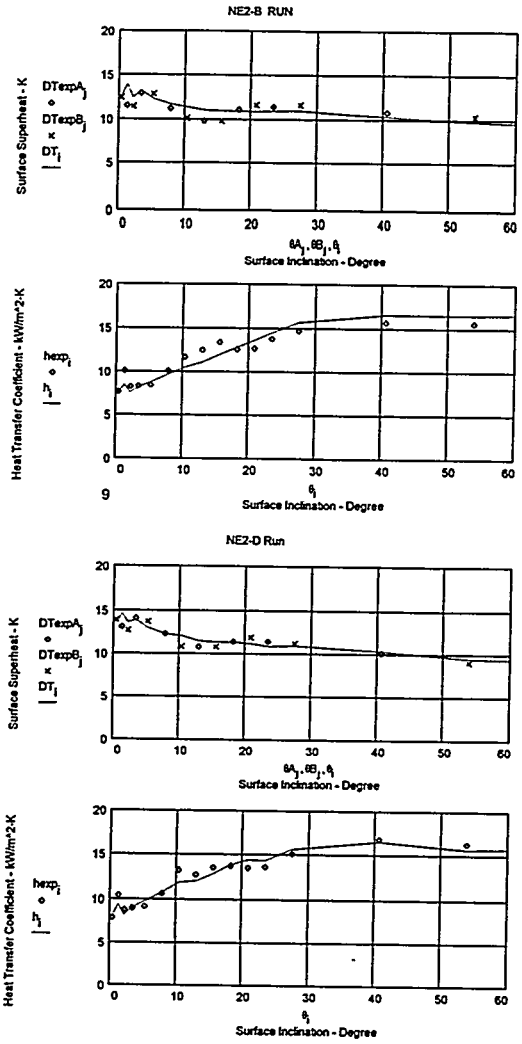

Figure 16. Comparison between the correlation and experimental data--surface superheat and heat transfer coefficient--edge-peaked heat flux cases.